Stable Operation of a Free-Electron Laser Driven by a Plasma Accelerator

M. Galletti,[1,2,3,*] D. Alesini,[4] M. P. Anania,[4] S. Arjmand,[4] M. Behtouei,[4] M. Bellaveglia,[4] A. Biagioni,[4] B. Buonomo,[4] F. Cardelli,[4] M. Carpanese,[5] E. Chiadroni,[4,6] A. Cianchi,[1,2,3] G. Costa,[4] A. Del Dotto,[7] M. Del Giorno,[4] F. Dipace,[4] A. Doria,[5] F. Filippi,[5] G. Franzini,[4] L. Giannessi,[4] A. Giribono,[4] P. Iovine,[8] V. Lollo,[4] A. Mostacci,[6] F. Nguyen,[5] M. Opromolla,[9,10] L. Pellegrino,[4] A. Petralia,[5] V. Petrillo,[9,10] L. Piersanti,[4] G. Di Pirro,[4] R. Pompili,[4] S. Romeo,[4] A. R. Rossi,[10] A. Selce,[5,11] V. Shpakov,[4] A. Stella,[4] C. Vaccarezza,[4] F. Villa,[4] A. Zigler,[4,12] and M. Ferrario[4]

[1]*Department of Physics, Università di Roma Tor Vergata, Via Ricerca Scientifica 1, 00133 Rome, Italy*
[2]*INFN-Tor Vergata, Via Ricerca Scientifica 1, 00133 Rome, Italy*
[3]*NAST Center, Via Ricerca Scientifica 1, 00133 Rome, Italy*
[4]*Laboratori Nazionali di Frascati, Via Enrico Fermi 54, 00044 Frascati, Italy*
[5]*ENEA Fusion and Technology for Nuclear Safety and Security Department (FSN), C.R. Frascati, via Enrico Fermi 45, 00044 Frascati, Italy*
[6]*Sapienza University, Piazzale Aldo Moro 5, 00185 Rome, Italy*
[7]*ENEA, C.R. Brasimone, 40032, Camugnano, Bologna, Italy*
[8]*INFN-Napoli, Via Cintia, 80126 Naples, Italy*
[9]*Università degli Studi di Milano, Via Celoria 16 20133 Milano Italy*
[10]*INFN-Milano, Via Celoria 16, 20133 Milan, Italy*
[11]*INFN-Roma Tre, Via della Vasca Navale 84, 00146 Roma RM, Italy*
[12]*Racah Institute of Physics, Hebrew University, 91904 Jerusalem, Israel*

(Received 2 August 2022; revised 25 October 2022; accepted 8 November 2022; published 29 November 2022)

The breakthrough provided by plasma-based accelerators enabled unprecedented accelerating fields by boosting electron beams to gigaelectronvolt energies within a few centimeters [1–4]. This, in turn, allows the realization of ultracompact light sources based on free-electron lasers (FELs) [5], as demonstrated by two pioneering experiments that reported the observation of self-amplified spontaneous emission (SASE) driven by plasma-accelerated beams [6,7]. However, the lack of stability and reproducibility due to the intrinsic nature of the SASE process (whose amplification starts from the shot noise of the electron beam) may hinder their effective implementation for user purposes. Here, we report a proof-of-principle experiment using plasma-accelerated beams to generate stable and reproducible FEL light seeded by an external laser. FEL radiation is emitted in the infrared range, showing the typical exponential growth of its energy over six consecutive undulators. Compared to SASE, the seeded FEL pulses have energies 2 orders of magnitude larger and stability that is 3 times higher.

DOI: 10.1103/PhysRevLett.129.234801

Light sources based on free-electron lasers (FELs) represent a fundamental tool to investigate the matter with atomic and subatomic resolution and at ultrafast timescales [8,9]. Their operation relies on the use of stable and high-energy (up to tens of GeV) electron beams that, to date, require the realization of accelerator facilities with large sizes and prohibitive costs. This is ultimately due to the limiting underlying accelerator technology, based on the use of radio-frequency (rf) waves with limited available accelerating fields [10]. Such a limit has been overcome by exploiting the huge fields that can be excited in a plasma [11] with pioneering experiments that demonstrated accelerating fields up to hundreds of GV/m, i.e., orders of magnitude larger than conventional rf technology [12–14]. Many works have then followed, motivated by the need to control the acceleration process and provide higher quality beams [15–18]. On this path, two proof-of-principle experiments have also demonstrated very recently that such a quality was sufficient to induce FEL lasing based on self-amplified spontaneous emission (SASE) [6,7]. However, with the amplification starting from an initial shot noise in the electron beam current, the stability and reproducibility of the emitted radiation are still not adequate to be adopted in user applications.

Here, we present the first proof-of-principle experiment demonstrating the stable generation of intense amplified radiation from a FEL driven by a centimeter-scale plasma accelerator. Using an external seed laser, FEL radiation is obtained at $\lambda_r \approx 827$ nm and improved in terms of output energy ($\approx$1.1 μJ) and stability (89%). Such enhancements are evident when comparing these results with the energies ($\approx$30 nJ) and stability (27%) we obtained in the SASE regime. The experiment has been performed at the SPARC_LAB test facility [19] using a beam-driven

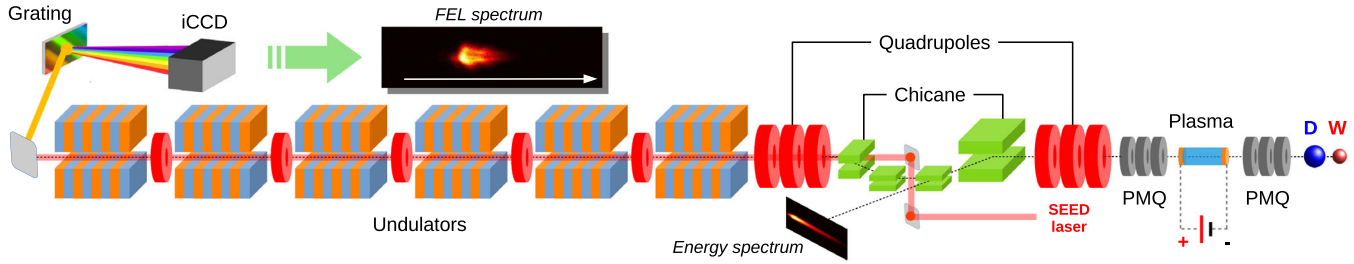

FIG. 1. Experimental setup. The driver (D) and witness (W) electron bunches, produced by the photoinjector, are focused by a triplet of PMQs in a 3 cm-long capillary containing the plasma produced by ionizing hydrogen gas with a high-voltage discharge. The accelerated witness is extracted by the second triplet of permanent-magnet quadrupoles (PMQs) and transported by using six electromagnetic quadrupoles. A magnetic chicane allows one to displace the beam and to insert an in-vacuum metallic mirror to inject the IR laser along the beam path. A dipole spectrometer is used to measure its energy with a scintillator screen installed on a 14° beamline. The FEL beamline consists of six planar undulators with tunable gaps and five quadrupoles in between. The emitted FEL radiation is collected by an in-vacuum high-reflective metallic mirror and measured with an imaging spectrometer equipped with a diffraction grating and a cooled intensified camera (iCCD).

plasma-wakefield accelerator (PWFA)[20] where the accelerating field, generated by a relativistic particle bunch acting as "driver," is used to accelerate a trailing "witness" bunch. The witness gains about 6 MeV energy over a 3 cm-long plasma and has low energy spread ($\approx 0.3\%$) and emittance (few microns). The 6D phase space of the accelerated beam is completely characterized, allowing a proper matching of the witness with a FEL beamline consisting of six planar undulators. Here, we observed the exponential growth and spectrum of the amplified light, confirming the typical features of the seeded FEL regime.

The experimental setup is shown in Fig. 1. Two ultrashort driver and witness electron bunches are generated by the SPARC_LAB photoinjector, consisting of an rf gun followed by three accelerating sections. A Ti:Sa laser system is employed to deliver ≈20 mJ energy pulses with 109 ± 10 fs (rms) duration at 10 Hz repetition rate. The main infrared pulse is split into two different lines. The first one, carrying most of the energy (tens of mJ), is converted to ultraviolet (266 nm) and used to generate the electron bunches on a copper photocathode [21]. The second low energy (hundreds of nJ) line is used to drive a single-shot nonintercepting electro-optical sampling (EOS) diagnostics [22] and the seed laser used for the FEL beamline. The bunches coming from the photoemission are then compressed down to a few tens of femtoseconds duration by tuning the first accelerating section at close-to-zero phase [23]. The beam diagnostics upstream of the plasma module consists of the EOS diagnostics station and, downstream of the plasma, an rf deflector and a magnetic spectrometer to characterize the time and energy profiles of the beam on a cerium-doped yttrium aluminium garnet (Ce:YAG) screen located after the spectrometer bending magnet [24].

The plasma accelerator module consists of a 3D-printed capillary with length $L_p = 3$ cm and 2 mm diameter. The capillary is filled with hydrogen gas through two symmetric inlets. The plasma is generated by ionizing the gas with a high-voltage discharge providing 5 kV pulses with 120 A current and ≈1 μs duration. For the experiment reported here, the plasma density is set to $n_e \approx 1.6 \times 10^{15}$ cm^{-3}. The stability and repeatability of the plasma formation are obtained by preionizing the gas with a neodymium-doped yttrium aluminum garnet (Nd:YAG) laser focused at the capillary entrance. This reduces the discharge timing jitter from tens to a few nanoseconds and, in turn, the plasma density fluctuations from 12% to 6% [25,26]. Two triplets of movable permanent-magnet quadrupoles (PMQs) are installed upstream and downstream of the capillary to focus the beam into the plasma and extract from it after acceleration [27].

The FEL beamline is made by six undulators, each one 2.15 m long with 77 periods with period $\lambda_u = 2.8$ cm and a magnetic chicane used to horizontally displace the beam and allow the injection of the seed laser on the same path. A quadrupole is installed between two consecutive undulators to transport the beam. The gap of each undulator can be tuned to adjust the undulator parameter in the range $K_u \approx 0.4 \div 3$. Downstream of each undulator, an in-vacuum metallic mirror can be inserted to send the FEL radiation to calibrated photodiodes. At the exit of the last undulator, the radiation spectrum is also measured with an imaging spectrometer equipped with a diffraction grating and a cooled intensified camera (iCCD). An imaging system consisting of a lens with a 30 cm focal length to make a magnification 3:1 of the FEL radiation at the spectrometer entrance slit (1.5 mm aperture) was used. The seed laser, with central wavelength $\lambda_L = 797 \pm 3$ nm and a 7 ± 1 nm (FWHM) bandwidth, has 24.2 ± 0.2 nJ energy with ≈250 fs (rms) duration. The laser is focused down to a ≈500 μm spot size at the entrance of the first undulator (≈25 μm transverse jitter) by means of a 5 m focal length lens. The divergence angle is about 0.2 mrad and the angular jitter is computed to be 0.15 mrad. A transfer line consisting of two motorized in-vacuum high-reflective mirrors is used to inject the seed laser into the FEL

beamline. A motorized delay line is then used to finely tune the delay between the seed laser and the plasma accelerated beam. By means of a photodiode and a CCD camera installed downstream of the last undulator, we performed a scan of the FEL pulse energy as a function of the seeding laser delay. When the two are temporally overlapped, an enhancement of the FEL energy is observed.

The experiment is performed by using driver and witness bunches separated by $\Delta t = 1.21 \pm 0.02$ ps. These are focused at the plasma entrance with the PMQs down to $\sigma_{r,d} = 20 \pm 1$ μm and $\sigma_{r,w} = 14 \pm 1$ μm, respectively. The driver charge is $Q_d = 200 \pm 5$ pC with duration $\sigma_{t,d} = 215 \pm 5$ fs. For the witness, the charge is $Q_w = 20 \pm 2$ pC and $\sigma_{t,w} = 30 \pm 3$ fs the duration. With the plasma turned off, the driver energy is $E_d = 87 \pm 0.1$ MeV with $\sigma_{E,d} = 0.23 \pm 0.01$ MeV energy spread, while for the witness $E_w = 86.6 \pm 0.1$ MeV and $\sigma_{E,w} = 0.31 \pm 0.02$ MeV. All the quantities are quoted as rms. The witness energy chirp is made positive (higher energy particles on the head) to compensate for the slope of the plasma wakefield and avoid the spoiling of the energy spread during acceleration [18]. The timing jitter between the seed laser and the electron beam measured by means of the EOS is approximately 50 fs.

The results discussed in the following are obtained in the quasinonlinear (QNL) regime [28], where the driver bunch density exceeds the plasma one and induces blowout but, due to its relatively small charge, the produced disturbance is linear. By defining $\tilde{Q} = N_b k_p^3 / n_p$ as the normalized bunch charge that quantifies the plasma response, with N_b the number of electrons contained in the driver and k_p the plasma wave number, such a regime is characterized by $\tilde{Q} < 1$, as opposed to the linear ($\tilde{Q} \ll 1$) and nonlinear (or blowout, $\tilde{Q} > 1$) cases. For the current configuration, it is $\tilde{Q} \approx 0.37$.

Figure 2(a) shows a single-shot energy spectrum of the driver and witness obtained with plasma turned off (top) and on (bottom) as detected at the cerium-doped yttrium aluminum garnet screen downstream of the magnetic spectrometer. The plot also shows the spectrum of the energy-depleted driver bunch that has been reconstructed by merging the images obtained with different currents of the magnetic spectrometer. Considering 500 consecutive shots of the accelerated witness, the resulting average energy is $E_w \approx 92.5 \pm 0.3$ MeV, corresponding to ≈ 200 MV/m accelerating gradient. On the contrary, the core of the driver bunch lost about 8 MeV in the plasma. The resulting energy spread of the accelerated witness is $\sigma_{E,w} = 0.31 \pm 0.08$ MeV, while its normalized emittance is $\epsilon_{x(y)} = 2.2 \pm 0.7 (1.8 \pm 0.2)$ μm. Numerical simulations have been performed with the ARCHITECT code [29] to support the experimental observations. The driver and witness bunches are thus propagated in a $L_p = 3$ cm-long plasma whose longitudinal profile resembles the experimental one,

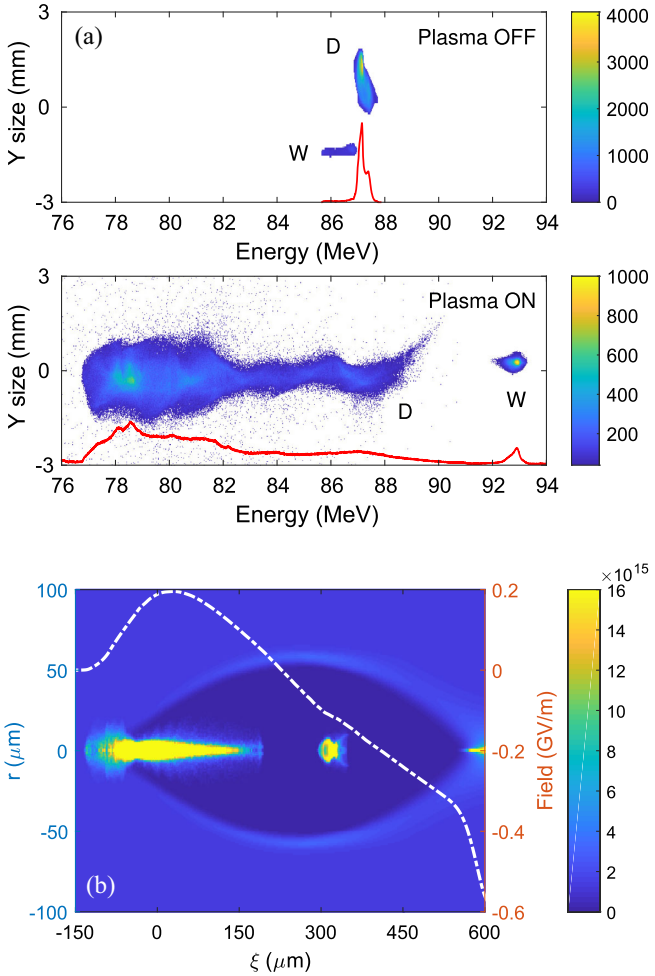

FIG. 2. Witness bunch acceleration in plasma. (a) Snapshot of the driver (D) and witness (W) spectrum with plasma turned off (top) and on (bottom). The red line shows the projected energy spectrum. The decelerated driver energy spectrum is obtained by merging the images obtained with different currents of the magnetic spectrometer. (b) Numerical simulation of the plasma wakefield acceleration. The snapshot shows the two bunches moving through the plasma background. The white dashed line shows the axial accelerating field along the longitudinal coordinate ξ.

measured offline with a Stark broadening-based diagnostics [30]. Figure 2(b) shows a snapshot of the two bunches propagating in the plasma background. The horizontal and vertical axes report the longitudinal (ξ) and radial (r) coordinates. The witness is located in the positively charged region produced by the driver and is accelerated with an average field of ≈ 200 MV/m, gaining approximately 6 MeV. The simulation confirms the energy gain and the preservation of the energy spread observed experimentally.

Downstream of the capillary, the beam is extracted by means of the second PMQ triplet and matched into the FEL beamline. At the entrance of the first undulator, the witness beam size is made ≈200 μm, with a transverse jitter of ≈20 μm. Passing through the undulators, the beam

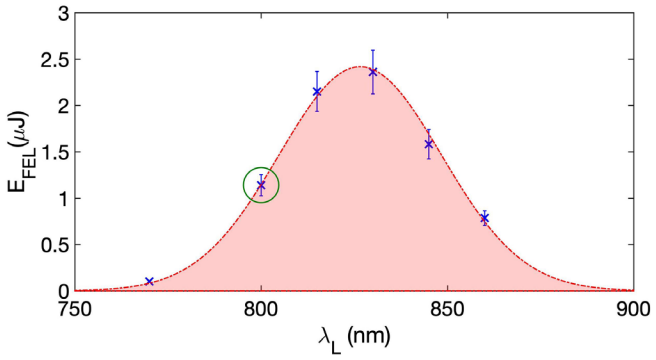

FIG. 3. Simulated FEL pulse energy (blue crosses) downstream of the last undulator as a function of the seed laser wavelength. The red dashed line shows the Gaussian fit of the theoretical data centered at 826.6 ± 4 nm. The green circle shows the expected energy for the seed wavelength used in the experiment.

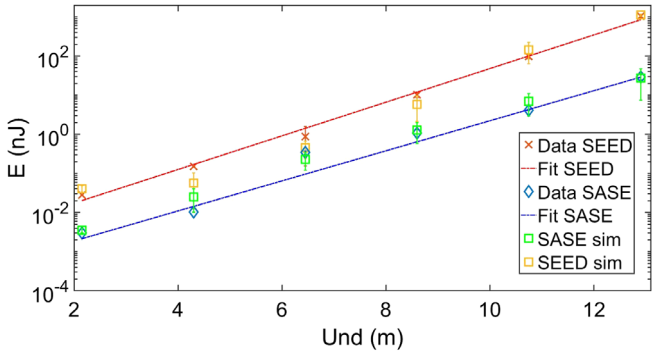

FIG. 4. Exponential growth of the radiation. Energy gain obtained with the seeded laser on and off along the undulators (red crosses and blue diamonds, respectively). The dashed lines show the exponential fit of the experimental data. The resulting FEL simulations (green and purple stars) are also reported. The error bars are computed as the standard deviation of the signal amplitudes measured at each point.

produces FEL radiation with spectrum peaked at a resonance wavelength $\lambda_r = \lambda_u(1 + K_u^2/2)/2\gamma^2 \approx 827$ nm, where γ is the relativistic Lorentz factor and $K_u \approx 1.35$. A proof of the light amplification along the undulators is provided by measuring the growth of the pulse energy after each undulator with the photodiodes. They collect the light emitted by the witness and driver since both bunches are transported through the undulators. The latter, however, has a much larger energy spread and is optically mismatched to the focusing-defocusing (FODO) lattice. This is sufficient to prevent light amplification from the driver alone, as it was verified by comparing the photodiode signal with and without the witness. The resonant wavelength of the FEL is set to be slightly different with respect to the seed one to be able to discriminate the two contributions from the retrieved spectrum traces. This does not prevent the amplification and stabilization of the FEL provided by the seed as shown in Fig. 3, which reports the expected energies downstream of the last undulator as a function of the seed laser wavelength. It is worth noting that for large wavelength separations the FEL pulse energy reduces to the SASE one.

To demonstrate the exponential growth of the radiation along the undulators' beamline and thus the effective amplification of the FEL radiation, we collected the light downstream of each undulator by using the calibrated photodiodes. Figure 4 shows the resulting energies (E_{pd}) measured as a function of the longitudinal coordinate (z) with the seed laser turned off (SASE regime) and on. At each point 200 consecutive shots were acquired, with the values reported corresponding to the average of the 30% more intense pulses. An average background signal resulting both from the seeding laser (when turned on) and the energy-depleted driver was separately measured by turning off the witness and then subtracted from the signal measured with it. The dashed lines show the numerical fit computed on the measured energies according to the exponential law $E_{\mathrm{pd}} = a \cdot \exp(z/L_g)$, with L_g the gain length. From the resulting fit, we have $L_g = 1.1 \pm 0.1$ m for SASE FEL and $L_g = 1.03 \pm 0.1$ m for the seeded FEL. The maximum energy gain achieved is $E_{\mathrm{pd}} \approx 30$ nJ in the first case and $E_{\mathrm{pd}} \approx 1.1$ μJ in the second one. The resulting brightness in this case is $(3 \pm 0.56) \times 10^{26}$ photons s^{-1} mm^{-2} mrad^{-2} 0.1% bandwidth $(\mathrm{BW})^{-1}$.

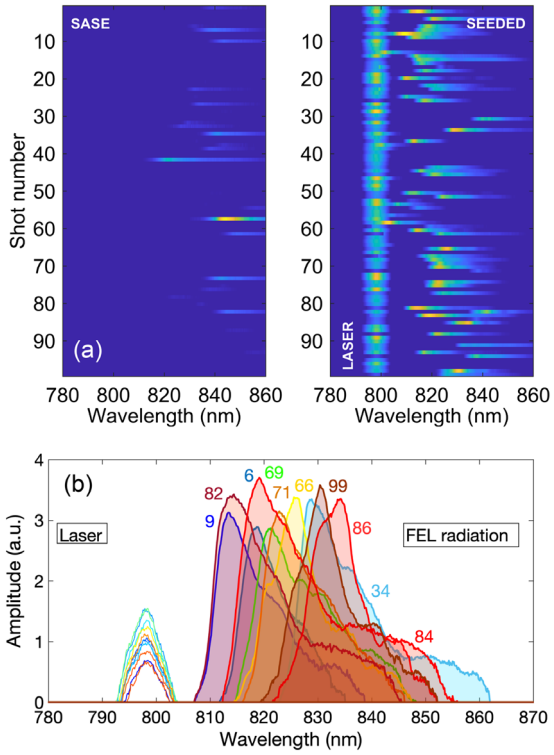

FIG. 5. Spectral analysis of the amplified light energy in the seeded configuration. (a) Comparison of 100 shots acquired in SASE and seeded FEL configurations with the seed laser turned off and on, respectively. (b) Spectral distributions of the 10 seeded FEL shots with the largest energies. The shot number is reported adopting the correspondent spectra color.

Both regimes highlight an exponential growth of about 4 orders of magnitude. Figure 4 also shows the numerical simulations obtained with the GENESIS1.3 code [31]. A set of 100 independent runs were processed similarly to the measured data by statistically varying the beam macroscopic parameters (charge, emittance, energy spread, and duration).

The single-mode amplification of light is also supported by the spectral measurements carried out with the imaging spectrometer, which collects the light at the end of the undulators' beamline. Figure 5(a) shows 100 consecutive shots acquired in SASE (left) and seeded (right) configuration (seed laser turned off or on, respectively). A clear enhancement of the radiation reproducibility is noticeable when using the seed laser, resulting in 89% of shots showing an FEL signal while in SASE it is 27%. The spectral distributions of 10 shots in the seeded configuration with the largest intensities are shown in Fig. 5(b). The FEL spectra present a single broad peak centered around the resonant wavelength, resulting $\lambda_r = 827 \pm 7$ nm, with $\sigma_\lambda = 4.5 \pm 1.2$ nm bandwidth. A similar result is obtained in the SASE configuration, with $\lambda_r = 826 \pm 9$ nm and $\sigma_\lambda = 4.7 \pm 1.1$ nm. Comparing the two regimes and considering only the shots showing FEL signals, the pulse energy rms fluctuation is 17% in SASE while it reduces to 6% in the seeded scheme.

In conclusion, we reported the first proof-of-principle experiment demonstrating stable and reproducible generation of coherent amplified FEL radiation driven by a centimeter-scale plasma accelerator. The obtained results indicate that the use of an external laser allows one to seed the emission process and to stabilize its amplification along six consecutive undulators. This strongly suppressed the fluctuations observed in previous experiments operating in the SASE regime. In view of the continuous efforts of the accelerator and plasma research community to develop next-generation ultracompact accelerators, these results represent a major breakthrough and they will contribute to their ultimate implementation in multidisciplinary facilities for user-oriented applications.

This work has been partially supported by the EU Commission in the Seventh Framework Program, Grant Agreement 312453-EuCARD-2, the European Union Horizon 2020 research and innovation program, Grant Agreement No. 653782 (EuPRAXIA), the INFN with the GRANT73/PLADIP grant, SL_COMB2FEL and PLASMAR Collaboration with ENEA FSN-FUSPHY Division. The work of one of us (A. Z.) was partially supported by PAZY Foundation.

*Corresponding author.
mario.galletti@lnf.infn.it

[1] S. P. Mangles *et al.*, Nature (London) **431**, 535 (2004).
[2] J. Faure, C. Rechatin, A. Norlin, A. Lifschitz, Y. Glinec, and V. Malka, Nature (London) **444**, 737 (2006).
[3] M. Litos *et al.*, Nature (London) **515**, 92 (2014).
[4] A. J. Gonsalves, K. Nakamura, J. Daniels, C. Benedetti, C. Pieronek *et al.*, Phys. Rev. Lett. **122**, 084801 (2019).
[5] K. Nakajima, Nat. Phys. **4**, 92 (2008).
[6] W. Wang, K. Feng, L. Ke, C. Yu, Y. Xu, R. Qi, Y. Chen, Z. Qin, Z. Zhang, M. Fang *et al.*, Nature (London) **595**, 516 (2021).
[7] R. Pompili *et al.*, Nature (London) **605**, 659 (2022).
[8] N. Hartmann *et al.*, Nat. Photonics **12**, 215 (2018).
[9] S. Pandey *et al.*, Nat. Methods **17**, 73 (2020).
[10] T. Argyropoulos, N. Catalan-Lasheras, A. Grudiev, G. Mcmonagle, E. Rodriguez-Castro *et al.*, Phys. Rev. Accel. Beams **21**, 061001 (2018).
[11] T. Tajima and J. M. Dawson, Phys. Rev. Lett. **43**, 267 (1979).
[12] A. Modena, Z. Najmudin, A. E. Dangor, C. E. Clayton, K. A. Marsh, C. Joshi, V. Malka, C. B. Darrow, C. Danson, D. Neely, and F. N. Walsh, Nature (London) **377**, 606 (1995).
[13] P. Sprangle, E. Esarey, and J. Krall, Phys. Plasmas **3**, 2183 (1996).
[14] I. Blumenfeld *et al.*, Nature (London) **445**, 741 (2007).
[15] A. Deng *et al.*, Nat. Phys. **15**, 1156 (2019).
[16] C. A. Lindstrom, J. M. Garland, S. Schroder, L. Boulton, G. Boyle *et al.*, Phys. Rev. Lett. **126**, 014801 (2021).
[17] M. Kirchen, S. Jalas, P. Messner, P. Winkler, T. Eichner, L. Hübner, T. Hülsenbusch, L. Jeppe, T. Parikh, M. Schnepp, and A. R. Maier, Phys. Rev. Lett. **126**, 174801 (2021).
[18] R. Pompili *et al.*, Nat. Phys. **17**, 499 (2021).
[19] M. Ferrario *et al.*, Nucl. Instrum. Methods Phys. Res., Sect. B **309**, 183 (2013).
[20] P. Chen, J. M. Dawson, R. W. Huff, and T. Katsouleas, Phys. Rev. Lett. **54**, 693 (1985).
[21] M. Ferrario *et al.*, Nucl. Instrum. Methods Phys. Res., Sect. A **637**, S43 (2011).
[22] R. Pompili *et al.*, New J. Phys. **18**, 083033 (2016).
[23] L. Serafini and M. Ferrario, AIP Conf. Proc. **581**, 87 (2001).
[24] A. Cianchi *et al.*, Phys. Rev. ST Accel. Beams **18**, 082804 (2015).
[25] A. Biagioni *et al.*, Plasma Phys. Controlled Fusion **63**, 115013 (2021).
[26] M. Galletti, M. P. Anania, S. Arjmand, A. Biagioni, G. Costa, M. Del Giorno, M. Ferrario, V. Lollo, R. Pompili, Y. Raz, V. Shpakov, F. Villa, A. Zigler, and A. Cianchi, Symmetry **14**450 (2022).
[27] R. Pompili *et al.*, Rev. Sci. Instrum. **89**, 033302 (2018).
[28] J. B. Rosenzweig, G. Andonian, M. Ferrario, P. Muggli, O. Williams, V. Yakimenko, and K. Xuan, AIP Conf. Proc. **1299**, 500 (2010).
[29] A. Marocchino, F. Massimo, A. R. Rossi, E. Chiadroni, and M. Ferrario, Nucl. Instrum. Methods Phys. Res., Sect. A **829**, 386 (2016).
[30] A. Biagioni *et al.*, J. Instrum. **14**, C03002 (2019).
[31] S. Reiche, Nucl. Instrum. Methods Phys. Res., Sect. A **429**, 243 (1999).